Available online at www.sciencedirect.com
ScienceDirect
Journal of Photochemistry and Photobiology A: Chemistry 187 (2007) 177–185
Journal of Photochemistry and Photobiology A:Chemistry
www.elsevier.com/locate/jphotochem

A novel scheelite-like structure of $BaBi_2Mo_4O_{16}$: Photocatalysis and investigation of the solid solution, $BaBi_2Mo_{4-x}W_xO_{16}$ ($0.25 \leq x \leq 1$)

B. Muktha [a], Giridhar Madras [b,*], T.N. Guru Row [a]

[a] *Solid State and Structural Chemistry Unit, Indian Institute of Science, Bangalore 560012, India*
[b] *Department of Chemical Engineering, Indian Institute of Science, Bangalore 560012, India*

Received 3 June 2006; received in revised form 12 September 2006; accepted 11 October 2006
Available online 10 November 2006

Abstract

A barium bismuth molybdate, $BaBi_2Mo_4O_{16}$, was synthesized for the first time. The compound was made by the solid-state technique and studied for photocatalytic degradation of water pollutants. The compound crystallizes in the monoclinic $C2/c$ system with $a = 5.317$ (1) Å, $b = 12.875$ (2) Å, $c = 19.390$ (3) Å, $\beta = 101.512$ (4)°, $V = 1327.1$ (4) Å^3 and $Z = 4$. The crystal structure along the a-axis consists of layers of $[Bi_2O_2]$ units and BaO_{10} polyhedra both surrounded by isolated MoO_4 tetrahedra representing a scheelite-like structure. Photocatalytic degradation of phenols and substituted phenols, acids and dyes were studied using $BaBi_2Mo_4O_{16}$ as catalyst. The catalyst shows selectivity towards chlorine containing aromatics. Substitution of tungsten for molybdenum resulted in retention of structure within the limits $0.25 \leq x \leq 1$ of the solid solution, $BaBi_2Mo_{4-x}W_xO_{16}$. The phases, $x = 0.25$, 0.50, 0.75 and 1.0, in the solid solution were also used to study the photocatalytic degradation of water pollutants like phenol, substituted phenols and dyes. The photocatalytic activity increases slightly with an increase in substitution of tungsten in the solid solution domain.

Keywords: Single crystal X-ray diffraction; Barium bismuth molybdate; Crystal structure; Photocatalysis; Phenols

1. Introduction

Selective catalytic oxidation and ammoxidation of olefins to corresponding diolefins, unsaturated aldehydes, acids and nitriles accounts for one-fourth of the industrial chemicals produced by the allylic oxidation proceses [1]. Bismuth molybdates are typical bimetallic oxide catalysts that are widely used for such reactions [2,3]. These catalysts are found to contain active sites capable of olefin chemisorption, ammonia activation, allylic intermediate, and lattice oxygen migration from the bulk to the surface active sites, dioxygen reduction, and incorporation of oxygen ions into anion vacancies into their structures [1]. As a result, bismuth molybdates like Bi_2MoO_6, $Bi_2Mo_2O_9$, and $Bi_2Mo_3O_{12}$ have been extensively studied for their catalytic activity [4–7]. A combination of these phases was found to enhance the selective oxidation of propylene to acrolein in what is termed as the "synergy effect" [8]. The well-known example for synergy effect is that of the co-operation between $Bi_2Mo_3O_{12}$ and Bi_2MoO_6 [9]. Substituted bismuth molybdates like $Bi_3FeMo_2O_{12}$ were found to be highly active and selective for oxidation of 1-butene to butadiene [10].

Among the three catalytically active bismuth molybdates, $Bi_2Mo_2O_9$, and $Bi_2Mo_3O_{12}$ are derivatives of fluorite structural type. $Bi_2Mo_2O_9$ has a fluorite related super structure with metal site vacancies: one of the every nine sites being absent [11]. $Bi_2Mo_3O_{12}$ can be described as a defective scheelite structure in which one out of every three Bi sites is vacant [12]. In both cases, the vacancies are in an ordered arrangement at room temperature within the infinite Bi channels. Bi_2MoO_6 shows polymorphism. The low temperature polymorph a rarely occurring mineral, koechlinite, belongs to the Aurivillius [13] family of oxides and is generally thought to be the catalytically active form since this is the stable bulk phase under reaction conditions (~650–750 K). Interestingly, the high temperature form [14] is the only fluorite derivative among the three bismuth molybdates with no vacant sites. Bi_2MoO_6 has been a subject of considerable attention and controversy due to its three-phase polymorphism [15].

Catalytic oxidation of olefins generally obeys the Mars and van Krevelen mechanism [16] based on redox cycle and the lattice oxide ion in the oxide bulk catalyst is an important

* Corresponding author. Tel.: +91 80 22932231; fax: +91 80 23600683.
E-mail address: giridhar@chemeng.iisc.ernet.in (G. Madras).

1010-6030/$ – see front matter © 2006 Elsevier B.V. All rights reserved.
doi:10.1016/j.jphotochem.2006.10.016

reaction participant at temperatures higher than 350 °C while gaseous oxygen re-oxidizes the catalysts [17]. The importance of high mobility of oxide ion was demonstrated in the $Bi_{1-3x}V_{1-x}Mo_xO_4$ system [18] using an ^{18}O tracer. Bi_2MoO_6 has the highest value of conductivity among the three phases described above and hence is a better catalyst owing to its role of transporting the active oxygen species to the surface. Scheelite-type $Na_{0.5-3x}La_{0.5+x}MoO_4$ [19] oxides with lattice ion mobility represent yet another class of compounds suitable for oxidation of olefins.

Kato et al. [20] studied the catalytic properties of semi conductor scheelite oxides (with band gaps more than 3.0 eV), using UV radiation. Photocatalytic splitting of water in the presence of $(NaBi)_{0.5}WO_4$ (in the presence of an electron donor) and $(NaBi)_{0.5}MoO_4$ and $(AgBi)_{0.5}MoO_4$ (both assisted by electron acceptors) were studied. So far, this is the only report of a bismuth molybdate used in a photocatalytic reaction.

The application of illuminated semiconductors for the degradation of the contaminants has been successfully used for a variety of compounds [21]. Our aim is to devise semiconductor bismuth molybdates to aid photocatalytic activity. In this context, we have synthesized a novel barium bismuth molybdate, $BaBi_2Mo_4O_{16}$, for the first time. The compound was further used to catalyze the photodegradation of dyes mainly used in the textile industry like Rhodamine (RB), Rhodamine blue (RBL) and industrial effluents like phenol and substituted phenols. Since W^{6+} can be substituted for Mo^{6+}, we have isolated a solid solution of the type, $BaBi_2Mo_{4-x}W_xO_{16}$ where $0.25 \leq x \leq 1$. In order to investigate the effect of tungsten substitution on photocatalytic activity, we have used these phases to degrade the dyes and substituted phenols.

2. Experimental

2.1. Materials

Bi_2O_3 (Fluka, 99.99%) was dried at 600 °C for 4 h prior to use. $BaCO_3$ (Fluka, 99.99%), MoO_3 (Fluka, 99.99%) and WO_3 (Fluka, 99.99%) were used as such. Phenol (P), 4-bromophenol (BP), 4-chlorophenol (CP), 2,4-dichlorophenol (DCP), 1,2,3,4,5-pentachlorophenol (PCP), 4-nitrophenol (NP), 4-chloro, 2-nitrophenol (CNP), 4-methoxy phenol (MOP), 4-methyl phenol (cresol) (MP) (all from Merck, India), acetic acid and mono chloroactetic acid (both from S.D. Fine-Chem Ltd., India) and the dyes Rhodamine blue (RBL, $C_{28}H_{32}N_2O_3$, CAS 1326-03-0) and Rhodamine (RB, $C_{28}H_{31}N_2O_3Cl$, CAS 81-88-9) (Rolex, India) were used as such. Water was double distilled and filtered through a Millipore membrane filter prior to use.

2.2. Synthesis

The compositions in the solid solution, $BaBi_2Mo_{4-x}W_xO_{16}$ were synthesized by the solid-state method using $BaCO_3$, Bi_2O_3, MoO_3 and WO_3 in stoichiometric quantities. The starting materials of all the compositions in the solid solution were ground well in an agate mortar. The reactant mixture corresponding to $BaBi_2Mo_4O_{16}$ was fired at 600 °C for 24 h and then the resultant mixture was intimately ground and re- fired at 600 °C for 24 h. A higher temperature was required for the syntheses of the tungsten substituted phases. The reaction mixtures of the compositions, $x = 0.25$, 0.50, 0.75 and 1.0 in the solid solution, $BaBi_2Mo_{4-x}W_xO_{16}$ were fired at 700 °C for 24 h and then were ground and re-fired at 700 °C for 24 h. Preliminary powder X-ray patterns of all the compositions confirmed the formation of a single phase in each case. Colorless single crystals of $BaBi_2Mo_4O_{16}$ were obtained by the melt cooling technique. The polycrystalline sample was heated at 900 °C for 1 h and then cooled at 1 °C/min up to 850 °C and then furnace cooled to room temperature. A part of the obtained single crystals were crushed and the powder X-ray pattern was recorded to establish the formation of a single phase.

2.3. Characterization

2.3.1. Powder X-ray diffraction

Powder X-ray diffraction data of all the phases were collected at room temperature on a Philips X' Pert Pro diffractometer, using Cu Kα radiation. Data were collected over the angular range $3^\circ \leq 2\theta \leq 120^\circ$ in steps of $\Delta(2\theta) = 0.01^\circ$. The X ray diffraction data were refined by a Le Bail profile analysis using the JANA2000 [22] program suite. The background was defined by the Chebsheyev polynomial function using 15 coefficients and the peak shapes were described by a pseudo-Voigt function varying five profile coefficients. For each diffraction pattern, a scale factor, a zero error factor, shape and unit cell parameters were refined.

2.3.2. Single crystal X-ray diffraction

Single crystal X-ray diffraction data were collected on a Bruker Axs SMART APEX CCD diffractometer [23] with a crystal to detector distance of 6.06 cm. The data were collected based on three sets of runs covering a complete sphere of reciprocal space with each set at different φ angle ($\varphi = 0$, 90 and 180°). Each frame covered 0.3° in ω. The data were reduced using SAINT PLUS [23] and the structure was solved by direct methods using SHELXS97 [24] and refined using JANA2000. Crystallographic data and the details of the single crystal data collection are given in Table 1.

The UV–vis diffuse reflectance spectra were recorded on a Perkin Elmer Lambda 35 UV–vis Spectrophotometer. DTA was performed on a SDTQ600 DSC/DTA instrument, under a constant flow nitrogen atmosphere. Thermo-gravimetric analysis of $BaBi_2Mo_4O_{16}$ indicates no weight loss on heating the sample over a temperature range from room temperature to 600 °C.

2.3.3. Photocatalytic experiments

2.3.3.1. Photochemical reactor. The photochemical reactor employed in this study comprised of two portions. The inner portion consisted of a jacketed quartz tube of 3.4 cm i.d., 4 cm o.d., 21 cm length and an outer pyrex glass reactor of 5.7 cm i.d., and 16 cm length. A high-pressure mercury vapor lamp (HPML) of 125 W (Philips, India) was placed after removal of the outer shell inside the jacketed quartz tube. The fluctuations in the input supply was controlled by a ballast and capacitor

Table 1
Crystallographic data for $BaBi_2Mo_4O_{16}$

Empirical formula	$BaBi_2Mo_4O_{16}$
Crystal habit, color	Cylindrical, colorless
Crystal size	0.086 mm × 0.131 mm × 0.248 mm
Crystal system	Monoclinic
Space group	*C*2/*c*
Cell dimensions	$a = 5.317$ (1) Å, $b = 12.875$ (2) Å, $c = 19.390$ (3) Å and $\beta = 101.512$ (2)°
Volume (Å^3)	1327.1 (4)
Formula weight	1345.54
Density (calculated) (g/cm^3)	5.979
Z	4
F(0 0 0)	2071
Scan mode	ω scan
θ range (°)	3.16–27.95
Recording reciprocal space	$-6 \le h \le 7$, $-16 \le k \le 16$, $0 \le l \le 15$
Number of measured reflections	5684
Number of independent reflections	1426 [R(int) = 0.0443]
μ (mm^{-1})	33.084
Number of refined parameters	36
$R(I > 4\sigma I)/R$ (all data)	0.0286/0.0286
$wR(I > 4\sigma I)/R$ (all data)	0.0693/0.0693
GoF	1.33
Max/min ($\Delta\rho$, E/Å^3)	1.093/−2.765

connected in series with the lamp. Water was circulated through the annulus of quartz tube to avoid heating of the solution ensuring that the reactions were carried out at 40 °C. The solution was taken in outer reactor and continuously stirred to ensure uniform suspension of the catalyst. The lamp radiated predominantly at 365 nm corresponding to the energy of 3.4 eV and photon flux is 5.8×10^{-6} mol of photons/s. Further details of the experimental setup can be found elsewhere [25].

2.3.3.2. Degradation experiments. The dyes/phenolic compounds were dissolved in double distilled Millipore filtered water. The degradation reactions were performed in a photochemical reactor with various initial concentrations with a constant catalyst concentration of 1.0 kg/m^3. Experiments were carried out with the compositions $x = 0.25$, 0.50, 0.75 and 1.0 in the solid solution, $BaBi_2Mo_{4-x}W_xO_{16}$, under similar conditions. Samples were collected at regular intervals for subsequent analysis. The samples were filtered through Millipore membrane filters and centrifuged to remove the catalyst particles prior to analysis, as described below. Control experiments conducted without the catalyst under UV radiation and with the catalyst, without UV radiation did not show any appreciable degradation indicating that both the catalyst and UV radiation are required for the degradation reactions. There was only about 1% reduction in the concentration of all compounds of interest when a solution of 100 ppm was stirred with the catalysts (at a loading of 1 kg/m^3) for 12 h in dark. Therefore, the actual concentration of the solution was taken to be the initial concentration for kinetic analysis. The optimal catalyst loading of the catalyst for 100 ppm of phenols was found to be 1 kg/m^3 with no significant increase in the degradation of organics for higher concentrations of the catalysts. Therefore, this catalyst concentration was used for all the photocatalytic degradation experiments. All these reactions were carried out at natural pH conditions. The initial concentration varied between 25 and 100 ppm for all phenols and between 5 and 20 ppm for the dyes owing to their high molar absorptivity (ε).

2.3.3.3. Sample analysis. The samples were analyzed by HPLC and the details can be obtained elsewhere [25]. HPLC analysis showed negligible amount of intermediates formed and the ratio of the absorption of the intermediates to the absorption of the parent compound was extremely small at initial degradation times (<10 min for 4-nitrophenol, 4-methylphenol and <30 min for other systems). Therefore, samples were only analyzed using Lambda 32, Perkin-Elmer UV–vis spectrophotometer to quantify the degradation reactions. The calibration for phenol, chlorophenols, 4-nitrophenol, 4-chloro-2-nitrophenol, 4-methoxy phenol, 4-methyl phenol, acetic acids, Rhodamine blue and Rhodamine were based on Beer–Lambert law at their maximum absorption wavelengths, λ_{max} of 270, 275, 320, 270, 285, 280, 200, 280, 547, 582, 270, 665 and 550 nm, respectively. Analysis of the samples using UV–vis spectrophotometer showed a continuous decrease in the UV–vis absorption at λ_{max} of the starting material confirming that there may be no interference by the intermediates formed, if any.

3. Results and discussion

3.1. Crystal structure

$BaBi_2Mo_4O_{16}$ crystallizes into the monoclinic system with $a = 5.317$ (1) Å, $b = 12.875$ (2) Å, $c = 19.390$ (3) Å, $\beta = 101.512$ (4)°, $V = 1327.1$ (4) Å^3 and $Z = 4$. The centrosymmetric space group *C*2/*c* was assigned based on the observed systematic absences. A numerical absorption correction was applied based on the cylindrical shape of the crystal. The positions of all the heavy (Bi, Ba and Mo) atoms were obtained by direct methods

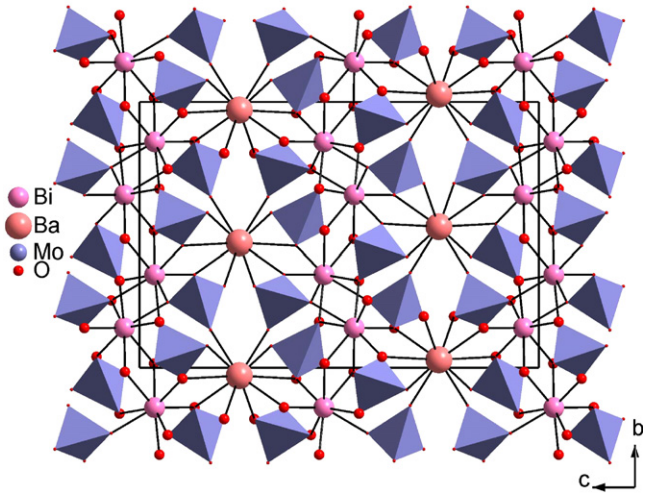

Fig. 1. Crystal structure of $BaBi_2Mo_4O_{16}$ along the *a*-axis.

Table 2
Selected bond distances of $BaBi_2Mo_4O_{16}$

Bi(1)–O(1)	2.382 (6)
Bi(1)–O(2)	2.436 (6)
Bi(1)–O(2′)	2.571 (6)
Bi(1)–O(3)	2.287 (7)
Bi(1)–O(7)	2.569 (6)
Bi(1)–O(7′)	2.332 (6)
Bi(1)–O(8)	2.563 (7)
Bi(1)–O(8′)	2.630 (7)
Mo(1)–O(1)	1.786 (6)
Mo(1)–O(2)	1.830 (6)
Mo(1)–O(6)	1.718 (7)
Mo(1)–O(8)	1.794 (7)
Ba(1)–O(1) × 2	3.046 (6)
Ba(1)–O(3) × 2	2.963 (6)
Ba(1)–O(4) × 2	2.698 (7)
Ba(1)–O(5) × 2	2.682 (7)
Ba(1)–O(6) × 2	2.969 (7)
Mo(2)–O(3)	1.812 (6)
Mo(2)–O(4)	1.718 (7)
Mo(2)–O(5)	1.731 (7)
Mo(2)–O(7)	1.838 (6)

and all the remaining oxygen atoms in the structure were located by difference Fourier synthesis. All the atoms occupy the general positions (8f sites) while Ba(1) occupies the 4e site. The final cycles of refinement led to a final *R* index of 0.028. The crystal structure along *a*-axis (Fig. 1) consists of layers of [Bi–O] units and BaO_{10} units separated by isolated MoO_4 tetrahedra. The structure can be regarded similar to the scheelite type, ABO_4. Fig. 2a shows the structure of monoclinic (space group *I*2/*b*) $BiVO_4$ [13], a typical example of the scheelite type. Both $BaBi_2Mo_4O_{16}$ and $BiVO_4$ have their unit cell parameters $a \approx a_F$ where a_F denotes the fluorite cell parameter. The variation of *b* and *c* unit cell parameters in $BaBi_2Mo_4O_{16}$ as compared to those of $BiVO_4$ is due to substitution of Ba. An expansion of the [Bi–O] units in both the compounds reveals the presence of the fluorite like $[Bi_2O_2]$ units (Fig. 2b and c). The presence of layers of isolated BaO_{10} polyhedral units in $BaBi_2Mo_4O_{16}$ is the only structural difference.

Bi(1) atoms in $BaBi_2Mo_4O_{16}$ is linked to eight oxygen atoms forming a $Bi(1)O_8$ polyhedron. It forms four short bonds (2.287–2.436 Å) with O(1), O(2), O(3) and O(7) and four relatively long bonds (2.563–2.630 Å) with O(2′), O(7′), O(8), and O(8′) atoms (Table 2). In general, bismuth molybdates depict a one-sided co-ordination due to the presence of the stereochemi-

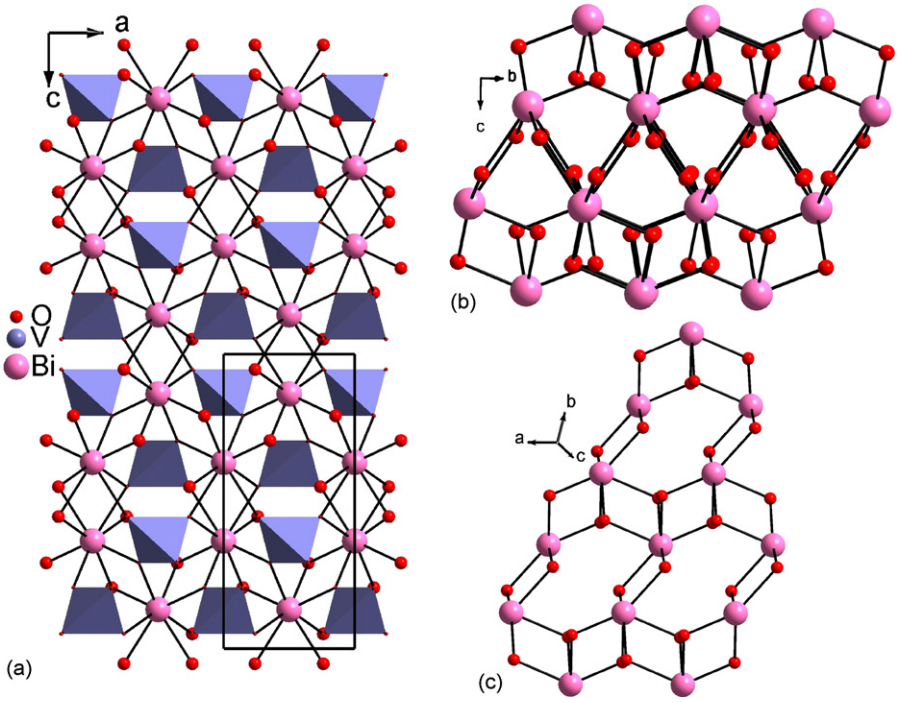

Fig. 2. (a) Crystal structure of $BiVO_4$ along *b*-axis. $[Bi_2O_2]$ units in (b) $BiVO_4$ and (c) $BaBi_2Mo_4O_{16}$.

cally active $6s^2$ lone pair of electrons. However the co-ordination of Bi(1) in this structure exhibits a well defined polyhedral arrangement. Each Bi atom is surrounded by eight MoO_4 tetrahedra. $Mo(1)O_4$ links to Bi atom through oxygen atoms O(2), O(8), their symmetry related atoms and O(1) while $Mo(2)O_4$ tetrahedra connects to Bi(1) through O(3), O(7) and O(7′) atoms. The layers of $[Bi_2O_2]$ units are connected to the BaO_{10} polyhedra via $Mo(2)O_4$ tetrahedra.

The structure consists of two types of MoO_4 tetrahedra. $Mo(1)O_4$ has bond distances in the range (1.718–1.830 Å) while the distances of $Mo(2)O_4$ range from (1.718–1.838 Å). The MoO_4 tetrahedra are not connected to each other. The displacement of the Mo atoms from the center of the tetrahedra is characterized by the difference in the Mo–O distances.

Ba(1) atoms form BaO_{10} polyhedra. It forms four short bonds with O(4) (2.698 (7) Å), O(5) (2.682 (7) Å) and their symmetry related atoms and six long bonds with O(1) (3.046 (6) Å), O(3) (2.963(6) Å), O(6) (2.969 (7) Å) and their symmetry related atoms. The atoms O(1) and O(6) and their symmetry related atoms of the BaO_{10} polyhedra are connected to $Mo(1)O_4$ tetrahedra while atoms O(3), O(4) and O(5) and their symmetry related atoms are connected to $Mo(2)O_4$ tetrahedra. The BaO_{10} units are linked to the MoO_4 tetrahedra only through the corners hence resulting in empty sites along the layer containing BaO_{10} units (Fig. 1). The BaO_{10} units are connected to Bi(1) via O(1) and O(3) atoms.

The powder X-ray patterns of the compositions, 0.25, 0.50, 0.75 and 1.0 in the solid solution, $BaBi_2Mo_{4-x}W_xO_{16}$ are shown in Fig. 3. The lattice parameters obtained from the single crystal X-ray data for the composition, $x = 0$, $BaBi_2Mo_4O_{16}$, were used to fit the profile for each powder pattern. The evolution of unit cell parameters a and c for the compositions in the solid solution is shown in Fig. 4. The unit cell parameter a decreases with an increase in the composition of tungsten. The c parameter shows an increase with an increase in composition of x. The b parameter does not show much variation. The volume

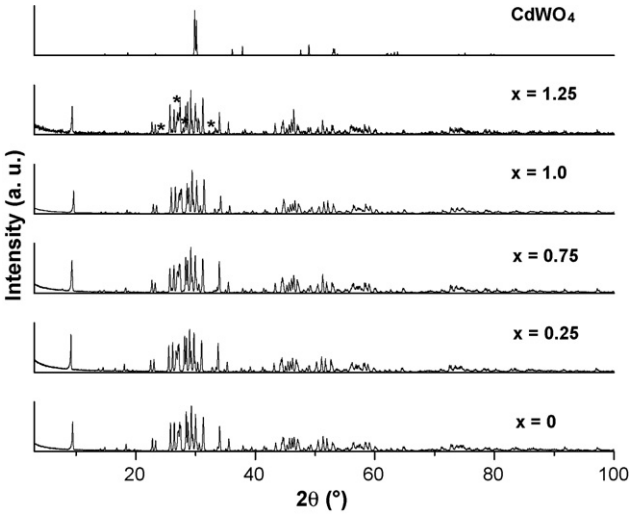

Fig. 3. Powder X-ray patterns of various members of the solid solution, $BaBi_2Mo_{4-x}W_xO_{16}$ and $CdWO_4$. The reflections marked with * for $x = 1.25$ represent impurities.

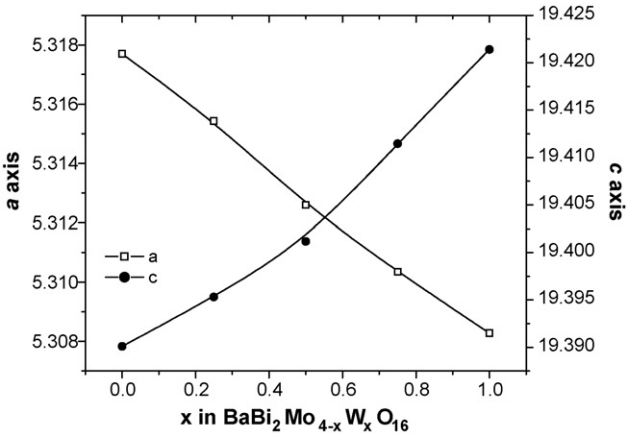

Fig. 4. Evolution of unit cell parameters in the solid solution, $BaBi_2Mo_{4-x}W_xO_{16}$.

decreases with an increase of the substitution of tungsten owing to the smaller ionic size of W^{6+} as compared to Mo^{6+}. The compositions beyond $x = 1$ indicate the appearance of multiple phases. Upon observation of the powder X-ray pattern of the composition $x = 1.25$, the major phase corresponded to that of $BaBi_2Mo_{2.75}W_{1.25}O_{16}$, while the minor impurity phases were related to bismuth molybdate, $Bi_{26}Mo_{10}O_{69}$ [26] and bismuth tungstate, $Bi_2W_2O_9$ [27] (Fig. 3). However, the minor phases do not disappear even on prolonged heating hence suggesting the limits of the solid solution between $x = 1$ and 0.25.

In the scheelite-type structure $CdMoO_4$, the substitution of W at the Mo site results in the wolframite structure [28]. The regular tetrahedral co-ordination for the B site atoms changes into an octahedral one and the structure exhibits waving chains of edge shared MoO_6 and WO_6 octahedra. However in $BaBi_2Mo_{4-x}W_xO_{16}$, interestingly, W^{6+} retains its tetrahedral co-ordination within the domain, as reflected by the powder X-ray patterns (Fig. 3), which show no change. Also, the powder pattern of the wolframite structure (Fig. 3) is very different from those of the phases in the solid solution, $BaBi_2Mo_{4-x}W_xO_{16}$. Increase in tungsten content results in appearance of several other phases however, the dominant phase corresponds to that of the phase, $BaBi_2Mo_4O_{16}$.

3.2. UV–vis spectra

The UV–vis spectra of the solid solution, $BaBi_2Mo_{4-x}W_xO_{16}$ are shown in Fig. 5. In order to obtain precise values of band gap from the absorption edges the point of inflection determined from the minimum in the first derivative of the absorption spectrum were used. Band gaps of 3.23 ± 0.02 eV for $x = 0.25$, 0.50, 0.75 and 1.0 in the solid solution, $BaBi_2Mo_{4-x}W_xO_{16}$ were obtained.

3.3. Photocatalysis

The photocatalytic degradation of two dyes, RB and RBL, was investigated. It was observed that RB did not show any degradation. In the presence of the catalyst $BaBi_2Mo_4O_{16}$,

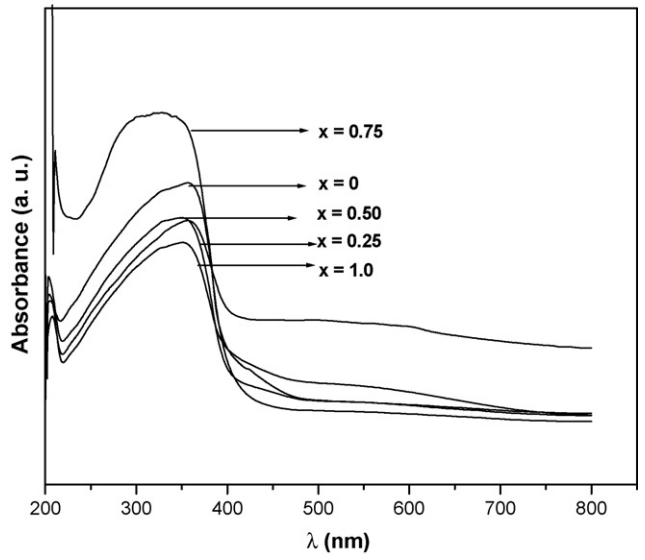

Fig. 5. UV–vis spectra of the members of the solid solution, $BaBi_2Mo_{4-x}W_xO_{16}$.

after 30 min of degradation of 25 ppm of RBL, the concentration decreased from 25 to 4 ppm. However, in the presence of Degussa P-25, after 30 min of degradation, the concentration of 25 ppm RBL decreased to ∼5.5 ppm [29]. The only structural difference between the two dyes is that RBL lacks chlorine in the structure. This suggested that the presence of chloro group in the structure of RB inhibited the degradation reaction with this catalyst. In order to further investigate this aspect, we considered the degradation of water pollutants such as chloro-substituted phenols and chloroacetic acid.

The degradation reactions of 25-ppm solutions of phenol (P), 4-chlorophenol (CP), 2,4-dichlorophenol (DCP) and 1,2,3,4,5-pentachlorophenol (PCP) with $BaBi_2Mo_4O_{16}$ were carried out (Fig. 6). In the presence of $BaBi_2Mo_4O_{16}$, after 30 min of degradation, the concentrations of 25 ppm solutions of P, CP, DCP

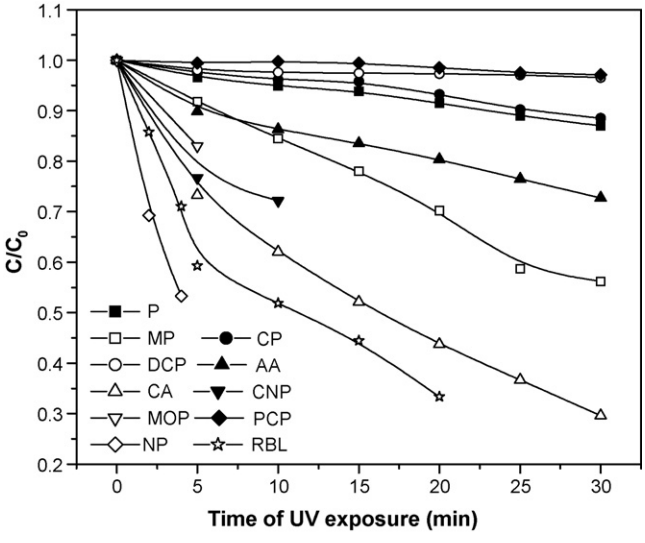

Fig. 6. Degradation profiles of 25 ppm solutions of RBL and various substituted phenols and acids by $BaBi_2Mo_4O_{16}$.

and PCP decreased to 23, 24, 24.5 and 24.8 ppm, respectively, while they decreased to 24.5, 22, 10 and 9 ppm, respectively, in the presence of Degussa P-25 titania [30]. This indicates that in the presence of $BaBi_2Mo_4O_{16}$, the degradation rate of chlorophenols is slower than that of phenol and follows the order, PCP < DCP < CP. This order is exactly the reverse of that observed during direct photolysis [31] or by photocatalytic degradation in the presence of titania [30]. To check whether the degradation of other substituted phenols (–Cl, $–CH_3$, $–NO_2$, etc.) also follow a different trend, the degradation of MP, MOP and NP was performed. In the presence of $BaBi_2Mo_4O_{16}$, after 5 min of degradation, the concentrations of 25 ppm solutions of NP [32] and MP [30] decreased to 11 and 22 ppm, respectively, while they decreased to 15 and 24 ppm, respectively, in the presence of Degussa P-25. These results indicate, in presence of $BaBi_2Mo_4O_{16}$, NP and MP degrade faster compared to the degradation in presence of titania. However, chlorophenols degrade slower in presence of $BaBi_2Mo_4O_{16}$ compared to the degradation in presence of titania. The degradation of 4-chloro 2-nitro phenol (CNP) was investigated to determine the effect of substituents on chlorophenol. However, the degradation of CNP is faster than that of chlorophenol (Fig. 6) because of the nitro substituent. Since chlorophenol degrades slower than phenol, and nitrophenol degrades faster than phenol, it seems to indicate that only the presence of chlorine in the structure hinders photocatalytic activity of these compounds.

To determine whether the chlorine substituent hinders degradation of aliphatic compounds, we investigated the degradation of acetic acid and chloroaceticacid. As shown in Fig. 6, the degradation is faster for chloroacetic acid than that of acetic acid. The degradation of chloroacetic acid being greater than that of acetic acid is consistent with the photocatalytic degradation in the presence of TiO_2 [33]. This can be explained on the basis of the mechanisms involved in both the degradation reactions. The degradation of chlorophenols proceeds via the free radical mechanism [20] while that of chloroacetic acid is through formation of chloride ions [33]. Thus experiments performed in this study indicate clearly that the compound, $BaBi_2Mo_4O_{16}$ is similar to TiO_2 in catalytic activity for all organics except for chlorine containing aromatics. However, the powder X-ray patterns before and after degradation did not show any change indicating no adsorption. Thus the reason for this selectivity is not apparent.

In order to quantify heterogeneous photocatalytic reactions [25] we used the first order rate expression, $r_0 = k_0 C_0$, where r_0 represents the initial rate, C_0 the initial concentration, k_0 denotes the kinetic rate constant. The linear dependency of initial rates, r_0, and initial concentrations, C_0, for all the substituted phenols and acids (Fig. 7a and b and Table 3) and RBL (Fig. 8a) confirm the first order kinetics of photocatalytic degradation of the selected range of compounds using $BaBi_2Mo_4O_{16}$. Fig. 7b shows the lower values of rate constants obtained for phenol (P), 4-chlorophenol (CP), 2,4-dichlorophenol (DCP), 1,2,3,4,5-pentachlorophenol (PCP) as compared to 4-methyl phenol (MP), 4-chloro, 2-nitrophenol (CNP), acetic acid (AA) and chloroacetic acid (CA) (Fig. 7b).

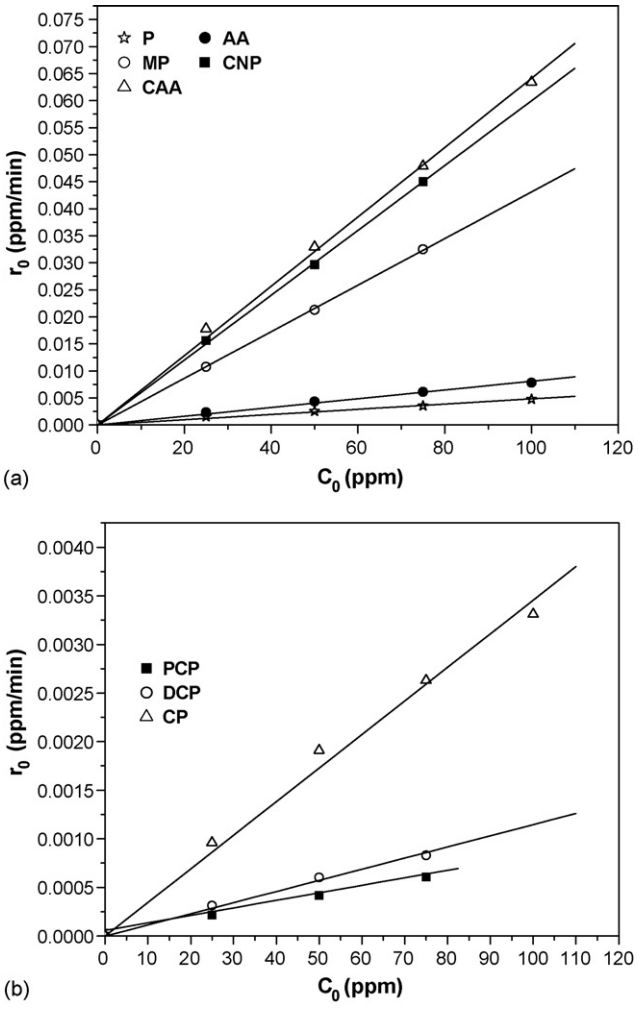

Fig. 7. (a) Variation of initial rates with concentration for photocatalytic degradation of phenols and acids by $BaBi_2Mo_4O_{16}$. (b) Variation of initial rates with concentration for photocatalytic degradation of chlorophenols by $BaBi_2Mo_4O_{16}$.

It is possibly interesting to compare the photocatalytic activity of this material with that of $BiVO_4$. $BiVO_4$ has been studied for the degradation of Rhodamine dye [34], phenol [35] and evolution of oxygen [36]. The photocatalytic activity of $BiVO_4$ has been attributed to the larger atom density of the basal (0 1 0) lattice plane on the exposed surfaces and the possible distortion of the Bi–O polyhedron [34]. However, $BaBi_2Mo_4O_{16}$, synthesized by the solid-state technique has negligible surface area. This indicates that the photocatalytic degradation is not a surface phenomenon. In photocatalysis, a frequently discussed issue is the oxidative pathway, i.e., direct hole attack or/and OH radical oxidation. In case of $BiVO_4$, no OH radicals are present in the phenol solution with $BiVO_4$ indicating that $BiVO_4$-mediated degradation of phenol occurs by the direct hole attack rather than by OH radical oxidation. Based on the observation of OH radical absence in the phenol and $BiVO_4$ system [35], it was suggested that the photo-generated electrons of $BiVO_4$ were captured by oxygen molecule and the degradation of phenol occured by the direct hole attack rather than by OH radical oxidation. However, the degradation of phenols by $BaBi_2Mo_4O_{16}$ shows the evolution of small amounts of intermediates, which were identified to be hydroxylated phenolic compounds by HPLC analysis. This indicates that the degradation of phenols occurs primarily through the OH radicals unlike that of $BiVO_4$. We hypothesize that the specificity of the photocatalytic degradation of chlorophenols can be attributed to the possibility of the

Table 3
First order initial photocatalytic rate constants for the degradation of pollutants in presence of $BaBi_2Mo_4O_{16}$

Pollutant	k ($\times 10^{-4}$ min^{-1})
Phenol	0.46
4-Chlorophenol	0.33
2,4-Dichlorophenol	0.11
2,3,4,5,6-Pentachlorophenol	0.08
4-Chloro,2-nitrophenol	5.96
4-Methylphenol	4.32
Acetic acid	0.77
Chloroacetic acid	6.27

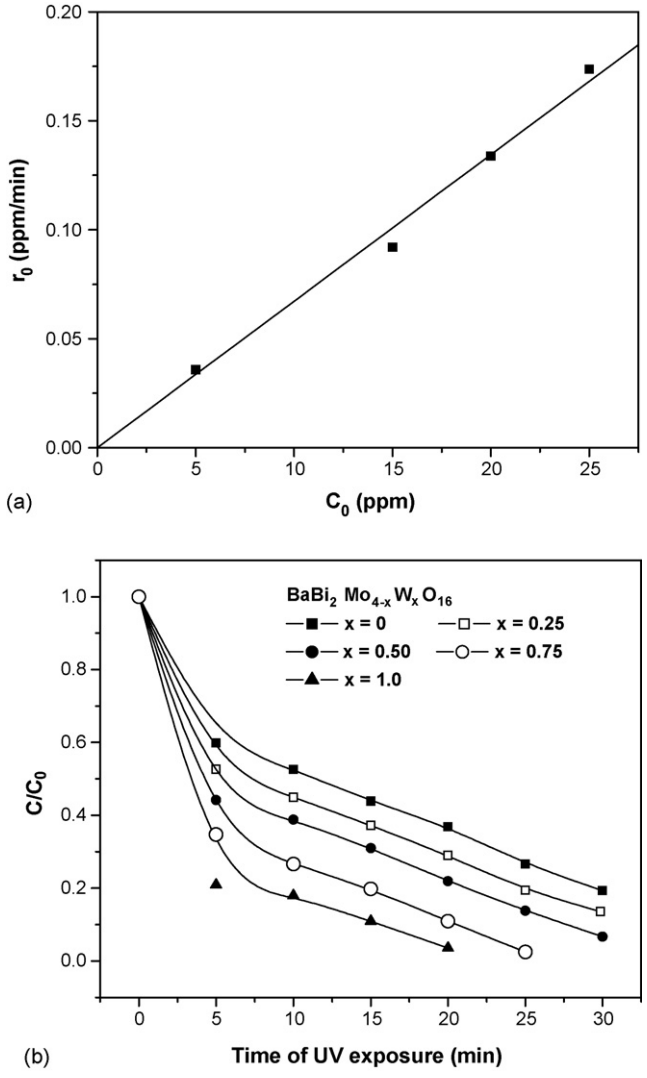

Fig. 8. (a) Variation of initial rates with concentration for photocatalytic degradation of RBL by $BaBi_2Mo_4O_{16}$. (b) The degradation profiles for compositions, $x = 0$, 0.25, 0.50, 0.75 and 1 in the solid solution, $BaBi_2Mo_{4-x}W_xO_{16}$.

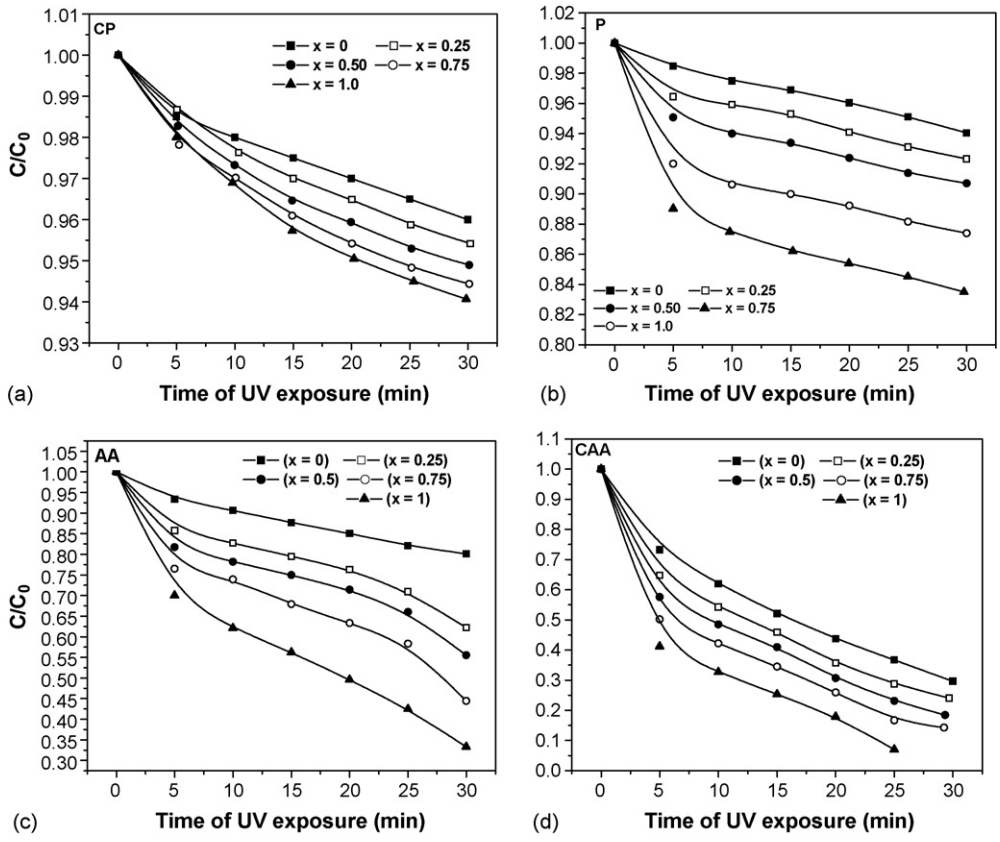

Fig. 9. (a–d) Photocatalytic degradation profiles of phenols and acids in presence of 1 kg/m^3 of compositions, $x = 0.25$, 0.50, 0.75 and 1.0 in the solid solution, $BaBi_2Mo_{4-x}W_xO_{16}$.

formation of a stable ligand between chlorophenol and Mo. The specificity for degradation is similar to that obtained in presence of $A_xBi_{26-x}Mo_{10}O_{68+0.5y}$ (A = Ba, $y = 0$; A = Bi, La, $y = 2$) [37].

The next objective of this work was to determine the effect of substitution of W^{6+} for Mo^{6+} on photocatalytic activity. The degradation of RBL (Fig. 8b), phenol (P), chlorophenol (CP), acetic acid (AA) and chloroacetic acid (CA) in the presence of $BaBi_2Mo_{4-x}W_xO_{16}$ with compositions $x = 0.25$, 0.50, 0.75 and 1.0 as catalysts was investigated. Fig. 9a–d shows the photocatalytic degradation profiles of the organics with various compositions. The degradation rates follow the same order as that of the parent compound, $BaBi_2Mo_4O_{16}$ (i.e. $x = 0$). However, the photocatalytic degradation rates are higher and increase with the substitution of tungsten for molybdenum even though the band gaps are similar.

Though the compositions of the solid solution, $BaBi_2Mo_{4-x}W_xO_{16}$ ($0 \le x \le 1$) have similar values of band gap, the molybdenum analogue shows the least activity. This implies differences in their electronic structures. In bismuth-(III) based semiconductors [38], the Bi 6s and O 2p orbitals form a hybridized valence band. In terms of this description, we assume that the valence band of $BaBi_2Mo_4O_{16}$ is composed of hybridized Bi 6s and O 2p orbitals, whereas the conduction band is composed of hybridized Bi 6p and Mo 4d orbitals and these bands meet the potential requirements of a photocatalytic oxidation. Since W atoms partially occupy Mo site, mixing of Mo 4d and W 5d valence orbitals should occur in the valence band of the tungsten substituted members of the solid solution, $BaBi_2Mo_{4-x}W_xO_{16}$ ($0 \le x \le 1$). The better photocatalytic activity may imply larger overlap of the hybridized orbitals of valence and conduction bands in the tungsten analogues than in $BaBi_2Mo_4O_{16}$.

4. Conclusions

A novel barium bismuth molybdate, $BaBi_2Mo_4O_{16}$ was synthesized and characterized by single crystal X-ray diffraction for the first time. The crystal structure depicts $[Bi_2O_2]$ units and BaO_{10} units surrounded by MoO_4 tetrahedra. The MoO_4 tetrahedra are not interlinked to each other and hence the compound is a poor conductor as is evident from the high band gap. Substitution of W^{6+} for Mo^{6+} results in a solid solution of the type, $BaBi_2Mo_{4-x}W_xO_{16}$ ($0.25 < x < 1$). An increase in tungsten content beyond $x = 1.0$, results in the appearance of additional phases with the retention of the scheelite-type structure. Selectivity towards chloro containing aromatics has been shown for the first time in $BaBi_2Mo_{4-x}W_xO_{16}$ ($0.25 < x < 1$). The degradation rates increase with the increase in substitution of tungsten in the solid solution. Despite similar band gaps, the tungsten analogues show higher activity than $BaBi_2Mo_4O_{16}$. This behavior may be attributed to larger overlap of the hybridized orbitals of valence and conduction bands in the tungsten analogues than in $BaBi_2Mo_4O_{16}$. All the compositions in the solid solution show specificity in degradation of phenolic compounds, dyes and acids. The degradation rates of 4-nitro phenol and 4-methyl

phenol in the presence of $BaBi_2Mo_4O_{16}$ catalyst are higher than those in the presence of TiO_2 catalyst whereas the rates of degradation of phenol and chloro phenols are lower than those for TiO_2 catalyst. Therefore it can be concluded that the catalyst, $BaBi_2Mo_4O_{16}$ is less active when the aromatic compound to be degraded has chlorine in its structure.

5. Supporting information available

CIF: the crystal data has been deposited at the Fachinformationszentrum Karlsruhe (FIZ) with the number CSD 416023.

Acknowledgements

Single crystal X-ray data collection on the CCD facility under the IRPHA-DST program, Indian Institute of Science is gratefully acknowledged. B. Muktha thanks CSIR for senior research fellowship.

References

[1] R.K. Graselli, Appl. Catal. 15 (1985) 127.
[2] R.K. Graselli, J. Burrington, Adv. Catal. 30 (1981) 133.
[3] Y.-M. Oka, W. Ueda, Adv. Catal. 40 (1994) 233.
[4] P.H.A. Batist, J.F.H. Bouwens, G.C.A. Schuit, J. Catal. 25 (1972) 1.
[5] T.-L. Kuo, D.-C. Wen, Appl. Catal. 142 (1996) 315.
[6] R. Rangel, P.-B. Bartolo, A.-G. Cartes, G. Diaz, S. Fuentes, D.H. Galvan, J. Mater. Syn. Proc. 9 (2001) 207.
[7] M.T. Le, J. van Craenenbroeck, I. van Driessche, S. Hoste, Appl. Catal. A: Gen. 249 (2003) 355.
[8] Z. Bing, S. Pei, S. Shishan, G. Xiexian, J. Chem. Soc., Faraday Trans. 86 (1990) 3145.
[9] D. Carson, M. Forissier, J.C. Vedrine, J. Chem. Soc., Faraday Trans. 84 (1980) 1017.
[10] W.J. Linn, A.W. Sleight, J. Catal. 41 (1976) 134.
[11] D.J. Buttrey, D.A. Jefferson, J.M. Thomas, Philos. Mag. A 53 (1986) 897.
[12] A.F.D. van Elzen, G.D. Rieck, Mater. Res. Bull. 10 (1975) 1163.
[13] B. Aurivillius, Ark. Kemi. 2 (1949) 519.
[14] D.J. Buttrey, T. Vogt, B.D. White, J. Solid State Chem. 155 (2000) 206.
[15] P.L. Gai, J. Solid State Chem. 49 (1983) 25.
[16] P. Mars, D.W. van Krevelen, Chem. Eng. Sci. 3 (1954) 41.
[17] L.D. Krenzke, W.J. Keulks, Catalysis 61 (1980) 316.
[18] W. Ueda, K. Asakawa, C.-L. Chen, Y.-M. Oka, T. Ikawa, J. Catal. 101 (1986) 360.
[19] Y.-H. Ho, W. Ueda, Y.-M. Oka, J. Catal. 186 (1999) 75.
[20] H. Kato, N. Matsudo, A. Kudo, Chem. Lett. 33 (2004) 1216.
[21] E. Pelizetti, C. Minero, P. Piccinini, M. Vincenti, Coord. Chem. Rev. 125 (1993) 183.
[22] V. Petricek, M. Dusek, JANA2000. Structure Determination Software Programs, Institute of Physics, Praha, Czech Republic, 2000.
[23] Bruker, SMART (Version 5.625), SAINT (Version 6. 45a) RLATT (Version 3. 0), Bruker AXS Inc., Madison, Wisconsin, USA, 2000.
[24] G.M. Sheldrick, SHELXS97. Program for Crystal Structure Solution, University of Gottingen, Germany, 1997.
[25] K. Nagaveni, G. Sivalingam, M.S. Hegde, G. Madras, Environ. Sci. Technol. 38 (2004) 1600.
[26] R.N. Vannier, G. Mairesse, F. Abraham, G. Nowogrocki, J. Solid State Chem. 122 (1996) 394.
[27] J.-C. Mesjard, B. Frit, A. Watanabe, J. Mater. Chem. 9 (1999) 1319.
[28] M. Daturi, L. Savary, G. Costentin, J.-C. Lavalley, Catal. Today 61 (2000) 231.
[29] T. Aarthi, G. Madras, Ind. Eng. Chem. Res., in press.
[30] G. Sivalingam, M.H. Priya, G. Madras, Appl. Catal. B: Environ. 51 (2004) 67.
[31] M. Czaplicka, J. Hazard. Mater. 134 (2006) 45.
[32] M.H. Priya, G. Madras, J. Photochem. Photobiol. A: Chem. 178 (2006) 1.
[33] A. Chemseddine, H.P. Boehm, J. Mol. Catal. 60 (1990) 295.
[34] L. Zhang, D. Chen, X. Jiao, J. Phys. Chem. B 110 (2006) 2668.
[35] B. Xie, H. Zhang, P. Cai, R. Qiu, Y. Xiong, Chemosphere 63 (2006) 956.
[36] S. Tokunaga, H. Kato, A. Kudo, Chem. Mater. 13 (2001) 4624.
[37] B. Muktha, T. Aarthi, G. Madras, T.N. Guru Row, J. Phys. Chem. B 110 (2006) 10280.
[38] H. Fu, C. Pan, W. Yao, Y. Zhu, J. Phys. Chem. B 109 (2005) 22432.